Molecular Characterization of Binding of Calcium and Carbohydrates by an Early Activation Antigen of Lymphocytes CD69†

Jiří Pavlíček,‡ Bruno Sopko,‡ Rüdiger Ettrich,§ Vladimír Kopecký, Jr.,‡,|| Vladimír Baumruk,|| Petr Man,‡,⊥ Vladimír Havlíček,⊥ Marek Vrbacký,▽ Ludmila Martínková,⊥ Vladimír Křen,⊥ Miloslav Pospíšil,⊥ and Karel Bezouška*,‡,⊥

Department of Biochemistry, Faculty of Science, Charles University in Prague, Hlavova 8, CZ-12840 Praha 2, Czech Republic, Laboratory of High Performance Computing, Institute of Physical Biology USB and Institute of Landscape Ecology AS CR, Zámek 136, CZ-37333 Nové Hrady, Czech Republic, Institute of Physics, Charles University in Prague, Ke Karlovu 5, CZ-12116 Praha 2, Czech Republic, Institute of Microbiology, Academy of Sciences of the Czech Republic, CZ-14220 Praha 4, Czech Republic, and Department of Pathological Physiology, 1st Medical Faculty, Charles University in Prague, U nemocnice 5, CZ-12853 Praha 2, Czech Republic

Received December 4, 2002; Revised Manuscript Received June 17, 2003

ABSTRACT: CD69 is the earliest leukocyte activation antigen playing a pivotal role in cellular signaling. Here, we show that a globular C-terminal domain of CD69 belonging to C-type lectins binds calcium through Asp 171, Glu 185, and Glu 187 with K_d ∼54 μM. Closure of the calcium-binding site results in a conformational shift of Thr 107 and Lys 172. Interestingly, structural changes in all of these amino acids lead to the formation of high-affinity binding sites for *N*-acetyl-D-glucosamine. Similarly, a structural change in Glu 185 and Glu 187 contributes to a high-affinity site for *N*-acetyl-D-galactosamine. Site-directed mutagenesis and molecular modeling allowed us to describe the structural details of binding sites for both carbohydrates. These studies explain the importance of calcium for recognition of carbohydrates by CD69 and provide an important paradigm for the role of weak interactions in the immune system.

CD69 is a signal transducing molecule of human leukocytes (*1*). It is constitutively expressed on $CD3^{bright}$ thymocytes (*2*), monocytes (*3*), neutrophils (*4*), epidermal Langerhans cells (*5*), and platelets (*6*) and induced very early after activation of T-lymphocytes, NK cells, and other cells of hematopoietic origin (*1*). CD69 is associated with a GTP-binding protein, and its rapid and transient surface expression from intracellular stores can be induced by cellular activation or heat shock independently of new RNA or protein synthesis (*7*).

CD69 is a disulfide-linked homodimer with two constitutively phosphorylated and variously glycosylated chains (*8*). It belongs to the type II integral membrane proteins possessing an extracellular C-terminal protein motif related to C-type animal lectins (*9*−*11*). Functional studies using a series of CD69/CD23 chimeras revealed the role of individual protein segments in this receptor. The transmembrane and cytoplasmic domains are responsible for signaling and cellular expression. The neck region of CD69 containing Cys 68 is important for receptor dimerization and proper surface expression. The globular protein segment corresponding to the carbohydrate recognition domain of C-type lectins (Ser 100 to Lys 199) mediates binding of most monoclonal antibodies used for receptor cross-linking. Moreover, this region, which is able to fuction independently of the rest of a CD69 antigen, is supposed to bind physiological ligands for this antigen (*12*).

The identification of physiological ligand(s) for CD69 is thought to be critical for uncovering molecular interactions that define its biology. Recent biochemical and structural investigations of several members of the group V C-type lectin-like receptors indicate that calcium, carbohydrates, peptides, and proteins can all be specific ligands (*13*−*17*). Since the sequencing of the CD69 receptor, it has been obvious that this protein cannot bind calcium in the way similar to the C-type lectin MBP. Only one amino acid from those that form two calcium-binding sites in MBP is conserved in CD69. The first structural consideration about the potential ligand-binding sites in CD69 comes from an early computer-based model (*18*). Two potential calcium-binding sites were suggested, but this prediction was not proved by recent crystal structures of this protein (*19*, *20*). However, in the paper by Natarajan et al. (*20*), an unknown

† This work was supported by Ministry of Education of the Czech Republic (MSM 113100001 and MSM 113200002), by Institutional Research Concept AV0Z5020903, by Grant Agency of the Czech Republic (524/00/1275 and 203/01/1018), and by Grant Agency of the Academy of Sciences of the Czech Republic (A7020006). Additional support was provided by the European Project BMH4-CT97-2671, including ERBIC20CT970022 (Czech Republic), and by Volkswagen Foundation (I-74679).

* To whom correspondence should be addressed. Tel.: +420-221 951 272. Fax: +420-221 951 283. E-mail: bezouska@biomed.cas.cz.

‡ Department of Biochemistry, Faculty of Science, Charles University in Prague.

§ Institute of Physical Biology USB and Institute of Landscape Ecology AS CR.

|| Institute of Physics, Charles University in Prague.

⊥ Academy of Sciences of the Czech Republic.

▽ Department of Pathological Physiology, 1st Medical Faculty, Charles University in Prague.

10.1021/bi027298l CCC: $25.00
Published on Web 07/15/2003

electron density in the area of Asp 171 and Glu 185 was detected, and a potential ligand-binding site involving this area was suggested. We have previously used recombinantly expressed soluble dimeric CD69 protein to identify calcium and certain carbohydrates such as *N*-acetyl-D-glucosamine and *N*-acetyl-D-galactosamine as the ligands for this protein (*21*). Using an alternative form of the soluble dimeric CD69, Childs et al. (*22*) failed to detect any interaction with the above-mentioned carbohydrates but observed a weak binding to the polysaccharide fucoidan. Surprisingly, structural studies of CD69 contributed little to solving the controversy. Molecular modeling studies (*18*) predicted the existence of cavity-shaped hydrophobic regions, one of which was supposed to be proximal to a potential low-affinity calcium-binding site and thus implemented in specific interactions of CD69 with its ligand. Recently, a crystal structure of the C-type lectin-like domain from human CD69 was determined by two different groups (*19*, *20*). While the former group noticed the existence of a hydrophobic patch surrounded by conserved charged residues constituting the probable ligand-binding site, the latter group concluded that a sugar-like density could represent, or mimic, part of the natural ligand recognized by CD69. To help to resolve the above controversies and to understand the molecular features responsible for ligand binding by CD69, we have initiated structural and binding studies using recombinant monomeric protein corresponding to the putative ligand-binding domain of CD69. Here, we present biochemical and structural data essential for understanding the structural elements involved in the recognition of calcium and carbohydrates by this receptor.

MATERIALS AND METHODS

Materials. Plasmid pCDA401 containing DNA coding the extracellular part of the CD69 molecule and the dimeric CD69 protein (CDA401) was described previously (*21*). All chemicals used in the experiments were high-grade commercial products. *N*-acetylhexosamines and their methyl glycosides were purchased from Sigma. The purity and anomeric composition was checked by 400 MHz ^{1}H NMR.[1] Commercial methyl-α-2-deoxy-2-acetamido-D-glucopyranoside was of insufficient purity and was thus synthesized in the laboratory. The radiolabeled compounds were from Amersham. [^{3}H]-*N*-Acetyl-D-galactosamine and [^{3}H]-*N*-acetyl-D-mannosamine not available commercially were synthesized according to the published procedure (*23*).

Expression, Refolding, and Purification of Wild-Type and Mutant CD69 Proteins. A DNA fragment encoding amino acid residues Ser 100 to Lys 199 of CD69 was amplified by polymerase chain reaction (PCR) from plasmid pCDA-401 (*21*) using 5′-TGTCTACTGTGAAGAGGAGCTGGACT-3′ as a forward primer and universal M13 primer as a reverse primer. The PCR fragment was digested with *Hind*III, phosphorylated using the T4 polynucleotide kinase, and ligated into the pET-30a(+) vector (Novagen) that had been opened by *Nde*I, filled with Klenow fragment, and digested with *Hind*III. Recombinant clones containing plasmid pCD69CWTY were selected for the recreation of the *Nde*I site. For the generation of point mutants, Quick Change Site-Directed Mutagenesis Kit (Stratagene) was used with pCD69CWTY as the template, and with the following oligonucleotide pairs: 5′-GTGAAGAGGAGCTGGGCT-TCAGCCCAAAATGCT-3′ and 5′-AGCATTTTGGGCT-GAAGCCCAGCTCCTCTTCAC-3′ for CD69CT1A; 5′-CGTTACAGGGCTTGCCAAGTGTGTTTTTCTG-3′ and 5′-CAGAAAAACACACTTGGCAGACCCTGTAACG-3′ for CD69CD1A; 5′-GTTACAGGGTCTGACGCGTGTGTTT-TTCTGAAA-3′ and 5′-TTTCAGAAAAACACACGCGT-CAGACCCTGTAAC-3′ for CD69CK1A; 5′-GGTCAG-CAGCATGGCATGTGAGAAGAATTTATACTG-3′ and 5′-CCAGTATAAATTCTTCTCACATGCCATGCTGCTGACC-3′ for CD69CE1A; 5′-GGTCAGCAGCATGGAATGTG-CGAAGAATTTATACTGG-3′ and 5′-CCAGTATAAAT-TCTTCGCACATTCCATGCTGCTGACC-3′ for CD69CE2A; and 5′-CGAT-ACGCAGGTAGAGCGGAACACTGGGT-TGGA-3′ and 5′-TCCAACCCAGTG-TTCGGCTCTACCT-GCGTATCG-3′ for CD69CE3A. All cloned inserts were sequenced on both strands using the dye T7 promoter primer with an automated DNA sequencer (ABI Prism 3100) according to the manufacturer's protocols.

For the production of proteins, expression plasmids were transformed into *Escherichia coli* strain BL-21 RIL (Stratagene). Bacteria were grown in 1 L Erlenmeyer flasks with 0.25 L of Luria broth at 37 °C. Induction was performed at an OD_{550} of 0.6 with 0.1 mM isopropyl-β-D-thiogalactopyranoside, and induced culture was grown for 5 h. Cells were harvested by centrifugation, and inclusion bodies were isolated (*24*). Inclusion bodies were dissolved in 50 mM Tris-HCl pH 8.0 with 6 M guanidine-HCl and 100 mM DTT, adjusted to 10 mg/mL protein, and centrifuged. One mL of clarified solution was added dropwise into 100 mL of the refolding buffer composed of 50 mM Tris-HCl pH 8.0, 0.5 M L-arginine, 1 mM $CaCl_2$, 0.1 mM PMSF, 1 μM leupeptine, 1 μM pepstatin, 1 mM NaN_3, 5 mM cystamin, and 3 mM cysteamin. The refolding mixture was dialyzed at 4 °C against 10 L of 10 mM Bis-Tris pH 7.0, 0.5 M NaCl, 1 mM NaN_3 and then twice against 10 L of 10 mM Bis-Tris pH 7.0, 29 mM NaCl, 1 mM NaN_3. The refolded CD69 protein was captured on a column of S-Sepharose FF (1.6 × 10 cm, Amersham) equilibrated in 10 mM Bis-Tris pH 7.0, 29 mM NaCl, 1 mM NaN_3. The column was eluted by linear gradient of NaCl from 29 mM to 2 M. Fractions containing CD69, as shown by SDS−PAGE, were concentrated by Centriprep device (Millipore), and monomeric proteins were isolated by chromatography on a Superdex 75HR column (1 × 30 cm, Amersham). Protein was dialyzed against 10 mM Hepes pH 7.0, 50 mM NaCl, 1 mM NaN_3 and concentrated to 10 mg/mL using Centriprep and a Centricon device (Millipore).

Characterization of CD69 Proteins. Wild-type and mutant CD69 proteins were characterized by SDS−PAGE under reducing and nonreducing conditions (*25*), by N-terminal sequencing from PVDF blots (*26*), and by MALDI mass spectrometry in linear and reflectron modes (*26*). Quantitations of these proteins were performed by quantitative amino acid analysis (AccuTag, Waters). For the complete verification of the primary structure including the disulfide bonding, wild-type and mutant CD69 proteins were digested with trypsin, and the tryptic fragments were separated by reverse

[1] Abbreviations: CD, circular dichroism; DTT, dithiothreitol; MALDI, matrix-assisted laser desorption/ionization; GlcNAc, *N*-acetyl-D-glucosamine; GalNAc, *N*-acetyl-D-galactosamine; ManNAc, *N*-acetyl-D-mannosamine; NMR, nuclear magnetic resonance; FTIR, Fourier transform infrared spectroscopy; PMSF, phenylmethylsulfonylfluoride; PVDF, polyvinylidenedifluoride; MBP, mannose-binding protein.

phase HPLC; the tryptic peptides were analyzed by MALDI mass spectrometry under conditions that preserve intact disulfide bridging of the cystine peptides (*26*). The proper refolding of CD69 proteins was checked by vibrational spectroscopy. Infrared spectra were recorded at room temperature with a Bruker IFS-66/S FT-IR spectrometer using a standard source, a KBr beam splitter, and an MCT detector. Usually 4000 scans were collected with 4 cm^{-1} spectral resolution and a Happ−Genzel apodization function. Samples of concentration in a range from 3 to 10 mg/mL were placed in a demountable cell (Graseby Specac) consisting of a pair of CaF_2 windows and a 12 μm Mylar spacer. Spectral contribution of a buffer in the carbonyl stretching region was corrected following the standard algorithm (*27*). Raman spectra were recorded in a standard 90° geometry on a multichannel instrument based on a 600 mm single spectrograph (1200 grooves/mm grating), a holographic notch-plus filter (Kaiser Optical Systems), and a liquid N_2 cooled CCD detection system (Princeton Instruments) having 1024 pixels along the dispersion axis. The effective spectral slit width was set to $\sim$5 cm^{-1}. Spectra were averaged from 300 exposures of 120 s each to produce the traces of highest quality. Samples in a capillary microcell (10 μL) were excited with a 514.5 nm line (100 mW) of an Ar^+ laser and kept at 4 °C. The spectra were treated according to ref *28*, and finally the spectra were smoothed using a 7-point Savitsky−Golay algorithm. CD spectra were measured using a Jasco J-600 spectropolarimeter equipped with a thermostated cell holder at 25 °C. Two μM solutions of the proteins were scanned in the far UV region (250−190 nm) in 10 mM phosphate buffer pH 7.4 in a 1 mm cell. The data were expressed as the mean residue ellipticity using the mean residue weight of 114.0 g/mol. The fraction content of the secondary structure elements was calculated using the procedure CONTIN with a set of 16 reference proteins.

Antigenic Analyses. Murine monoclonal antibodies were against CD69, clones MLR3 (gift of Dr. Angela Risso, University of Udine, Italy), Leu23 (Pharmingen BD), and BL-Ac/p26 (gift of Dr. Jorg Hamann, University of Leipzig, Germany); all three were conformation-sensitive and recognizing native CD69 and clone BL-KFB/B1 (gift from Dr. Jorg Hamann) that binds to native as well as denatured CD69. Antibodies against rat NK cell receptor NKR-P1 (clone 3.2.3., Harlan) were used as a negative control. For binding experiments, 1 μg of wild-type or mutant CD69 proteins in 50 μL of 10 mM phosphate buffer pH 7.4 with 0.15 M NaCl (PBS) was added to triplicate wells (Immulon 4, Dynatech) and incubated at 4 °C for 16 h. Wells were washed with PBS, blocked with 1% BSA in PBS, and incubated with primary murine antibodies (10 μg of protein/mL) at the indicated temperature for 6 h. Binding of the primary antibody was detected to washed wells after incubation with goat anti-mouse immunoglobulin labeled with $Na^{125}I$ (specific activity 10^6 cpm/mg protein) for 30 min and then a final washing with PBS by liquid scintillation counting of individual wells (Microbeta, Wallac). Protein in control wells was denatured with 6 M guanidine-HCl and 10 mM DTT for 1 h prior to washing and incubation with the primary antibodies.

Recalcification and Complete Decalcification of CD69CWTY. CD69CWTY was fully recalcified by incubation in TBS buffer (Tris-buffered saline, 10 mM Tris-HCl pH 7.5, 150 mM NaCl) containing 10 mM $CaCl_2$, followed by extensive dialysis of the protein against calcium-free TBS buffer. To investigate calcium saturation of CD69 under physiological conditions, 1 mL of CD69CWTY (1 mM) was saturated with calcium and dialyzed for 30 h against 1 L of TBS with 1 mM $CaCl_2$. The concentration of calcium inside the dialysis bag was monitored after 1, 3, 5, 10, 15, 20, 25, and 30 h using a tracer amount of $^{45}CaCl_2$. Calcium-free CD69CWTY was prepared in a similar way by extensive dialysis against acidic buffer, pH 3.5.

Plate Binding and Inhibition Assays. Plate binding and inhibition studies were performed as described previously (*29*). Briefly, microtiter wells Immunol 4 (Dynatech) were coated overnight with 10 μg/mL solutions of $GlcNAc_{23}$BSA (Sigma) in TBS buffer pH 7.4 (10 mM Tris-HCl, 0.15 M NaCl, 1 mM NaN_3). Wells were washed three times with TBS buffer and blocked with 1% BSA in TBS buffer for 2 h at 4 °C. CD69CWTY protein was radiolabeled with $Na^{125}I$ (Amersham). The radiolabeled protein was diluted with 2% BSA in twice-concentrated TBS buffer to specific activity 100 000 cpm/mL and mixed in duplicates with the inhibitory saccharides serially diluted in water. These mixtures were transferred to blocked coated wells and incubated for 2 h at 4 °C, then wells were washed four times with cold TBS buffer, and the radioactivity bound to individual wells was counted directly in the plate (Microbeta, Wallac) after the addition of the scintillant.

Equilibrium Dialysis. Equilibrium dialysis was performed as described previously (*30*). Defined concentrations of wild-type or mutant CD69 monomeric proteins in TBS buffer (10 mM Tris pH 7.5 with 130 mM NaCl and 1 mM NaN_3) were placed into a 100 μL compartment, while the radiolabeled ligands in TBS buffer (diluted to the required specific activity with the unlabeled ligands when necessary) were placed into a 1 mL compartment. The two compartments were separated by SpectraPore tubing with molecular weight cutoff of 3000. Both compartments were rotated at 50 rpm in the cold room (4 °C) for 24 h necessary to establish the equilibrium. Thereafter, 10 μL samples were taken from both compartments for the determination of radioactivity by liquid scintillation counting (^{45}Ca has a spectrum similar with ^{33}P that was used without any correction). The binding data were evaluated using a Scatchard plot. If only one class of binding sites is present, this plot is linear, the intercept on the abscissa gives the number of binding sites per mol of the protein, and the slope gives $-1/K_d$, where K_d is the dissociation constant for the interaction of ligand with the protein. If binding sites of unequal affinity for the ligand are present, the plot takes the form of a hyperbola. For two classes of binding sites, the asymptotes have slopes equal to $-1/K_d$ for each class of site, and the intercepts on the abscissa give the two values for the number of binding sites. The intercept between the curve and the abscissa is equal to the total number of binding sites (*31*).

Molecular Modeling. The structure (1E87) was extracted from the Brookhaven Protein Data Bank (http://www.pdb.org) and loaded into SYBYL 6.6.2 (Tripos Associates), where we extracted a shortened construct from Ser 100 to Lys 199. Hydrogens were added, and a Conolly type surface with the electrostatic potential based on Gasteiger−Hückel partial charge distributions was calculated. A potential binding site for calcium on the surface was identified by the

fact that the coordination of a calcium ion demands a negatively charged region. The positioning of the calcium ion in this site was done with the DOCK module included in SYBYL/MAXIMIN2 that calculates energies of interaction based on steric contributions from the TRIPOS force field and electrostatic contributions from any atomic charges present in the ligand. After positioning the ion, the whole protein was solvated in a precomputed water box of tip water (two layers), and periodic boundary conditions were applied to maintain solvent density. The solvent−protein system was minimized by 100 iterations with the Powell minimizer and the TRIPOS force field including electrostatic interactions based on Gasteiger−Hückel partial charge distributions using a dielectric constant with a distance-dependent function $\epsilon = 4r$ and a nonbonded interaction cutoff of 8 Å (*32*, *33*). The minimization was followed by a molecular dynamics simulation at 290 K with the NTV ensemble over 15 000 fs. The resulting structure was then minimized with the same parameters as above to convergence of the energy gradient less than 0.01 kcal mol^{-1} Å^{-1}.

The interactions with ligands were studied using the AutoDock 3.0.3 program. AutoDock (*34*) is a program suite for automated docking of flexible ligands to receptors. To allow flexibility of the ligand, bonds were assigned as rotatable with the deftors program. Grid maps with 120 grid points in each direction and a grid point spacing of 0.2 Å for each atom type present in GlcNAC were calculated using AutoGrid. In addition to the atomic-affinity grid maps, AutoDock requires an electrostatic potential grid map, calculated by solvation of the linearized Poisson−Boltzmann equation. For the explicit modeling of hydrogen bonds, it was necessary to add polar hydrogens and assign partial atomic charges to the macromolecule. For the docking the Lamarckian Genetic Algorithm (GA-LS), a hybrid search technique that implements an adaptive global optimizer with local search (*35*) was used. The exploration of docking positions included for every arbitrary position 50 hybrid GA-LS docking runs using a population size of 50, a maximum number of energy evaluations of 25 000, a maximum number of generations of 27 000, and 300 iterations of a Solis and Wets local search. The resulting positions were clustered according to a RMS criterion of 1 Å, and the most energetically favorable position of every cluster was visually analyzed. The selected docking positions were subjected to 2000 steps of steepest descent minimization optimizing both internal and relative geometries of the substrate and the binding-site residues. After solvatation of the complex, a molecular dynamics simulation followed by minimization was performed with same parameters as described above for the docking of calcium. The nonbonded interaction energy between the antigen and the ligand within the resulting structure was calculated using the TRIPOS force field. This estimation of the real interaction energy neglects solvatation and desolvatation effects; however, this shortcoming is minimized by the molecular dynamics simulation in the solvent that shows that these effects do not significantly change the positions of the ligands during the binding.

RESULTS AND DISCUSSION

Expression, Purification, and Characterization of the Recombinant Proteins. We have previously produced recombinant CD69 from fusions with the maltose-binding protein. However, since the original protocol would be too laborious to generate sufficient supplies of wild-type and several mutated proteins, we have evaluated alternative expression constructs. Since the ligand domain of CD69 has been defined in the recent domain swap experiments (*12*), we prepared constructs limited to the C-terminal portion including residues 100−199 (Figure 1A, CD69CWTY) and used previously described dimeric CD69 as a reference. The new construct would produce a minimal size monomeric protein known to contain all amino acid residues responsible for the binding of calcium and carbohydrates (*21*). A DNA

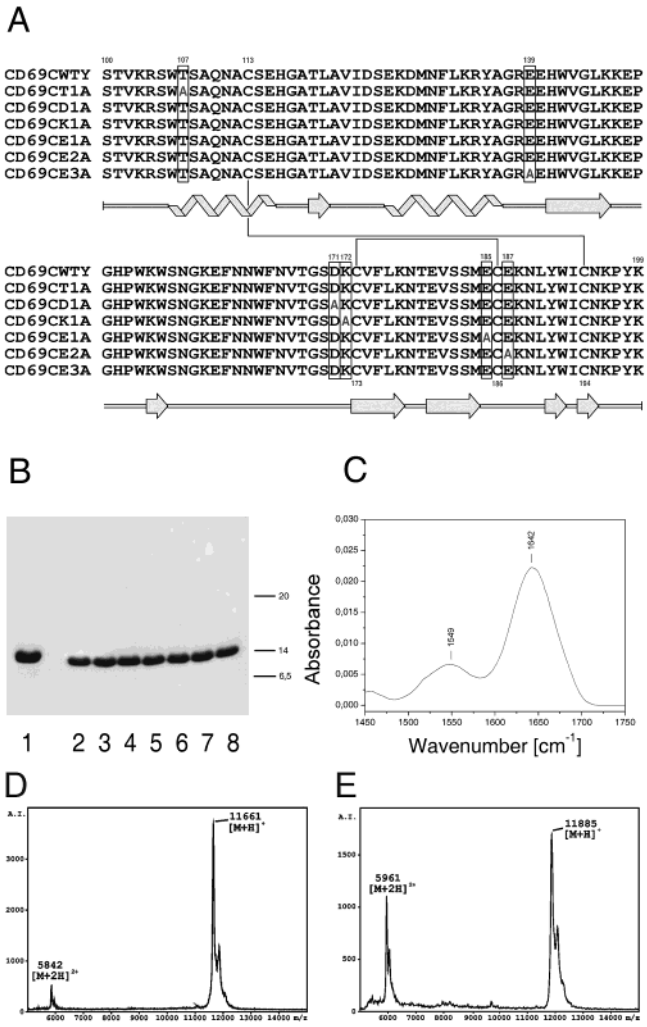

FIGURE 1: Schematic description of the CD69 constructs used in the study. (A) The expression constructs used for the production of the recombinant CD69 (residues 100−199). Proteins in which certain amino acids have been mutated to alanine include those with mutated Asp 171 (D1A protein), Lys 172 (K1A protein), Glu 185 (E1A protein), Glu 187 (E2A protein), and Glu 139 (E3A protein). Elements of secondary structure are schematically indicated together with the disulfide bond found in CD69. (B) Analysis of the refolded proteins by SDS−PAGE. Protein markers were soya trypsin inhibitor (20 kDa), lysozyme (14 kDa), and aprotinin (6.5 kDa). Lanes 1 and 2 contains CD69CWTY under reducing (1), and nonreducing (2) conditions. Lanes 3−8 contain CD69CT1A, CD69CD1A, CD69CK1A, CD69CE1A, CD69CE2A, and CD69CE3A, respectively, all under nonreducing conditions. Gels were stained by Coomassie Brilliant Blue R-250, and 5 μg of protein samples was applied. (C) FTIR spectrum in the region from 1450 to 1750 cm^{-1} corresponding to the amide I and II bands of protein CD69CWTY, 5 mg/mL. (D and E) MALDI spectra of CD69CWTY treated with iodoacetamide and with DTT and iodoacetamide, respectively.

fragment coding this domain was inserted into the prokaryotic expression vector pET-30a(+) just after triplet coding for the initiation methionine. The resulting proteins could be obtained in good yield (0.6−1.4 mg/1 L of induced bacterial culture, as shown by quantitative amino acid analyses). SDS polyacrylamide electrophoresis under reducing conditions (Figure 1B, lane 1) and MALDI mass spectrometry both demonstrated high purity of the prepared proteins. N-terminal sequencing revealed that this protein was produced in the native form devoid of the initiation methionine. Molecular mass (CD69CWTY, $[M + H]^+ = 11597$, not shown) examined by MALDI mass spectrometry provided additional confirmation of the identity and integrity of the protein. The spectra displayed the presence of only one compound and its doubly charged form corresponding to our construct. On SDS−PAGE under nonreducing conditions, a single protein band with the mobility shifted toward the cathode was observed, indicating homogeneous disulfide bonding in the protein (Figure 1B, lane 2). Additional evidence for the proper closing of two disulfide bonds was obtained by chemical modification of the entire protein. Considering the mass accuracy of MALDI mass spectrometry (±20 Da), treatment with iodacetamide did not result in any measurable change of the molecular mass indicating no free cysteine residues (see an example for CD69CWTY, $[M + H]^+ = 11\,661$, Figure 1D). The combined treatment by both reducing agent (DTT) and iodacetamide led to a mass shift of 224 Da corresponding to four acetamidations of cysteines generated by the reduction of two disulfide bonds in the protein (cf. Figure 1D,E). Final evidence for the unique pairing of disulfides was obtained by MALDI mass spectrometry of tryptic digests. Complete coverage of the sequence by tryptic peptides allowed us to identify the two cystic peptides corresponding to residues [74−78]-S−S-[79−89] and residues [5−28]-S−S-[90−100]. These peptides confirm the disulfide pairing shown in Figure 1A. Mutant CD69 proteins (Figure 1A) were produced refolded and analyzed under identical conditions (Figure 1B, lanes 3−8).

The monomeric status of all CD69 proteins was confirmed by gel filtration analysis on a Superdex 75 column. The evaluation of the proper folding of wild-type and mutant CD69 proteins was a prerequisite for the subsequent experiments. However, verification of folding for all seven proteins produced here by protein crystallography or NMR experiments would be complicated and time-consuming. Therefore, we used spectroscopical techniques such as circular dichroism and infrared or Raman spectroscopy that can, in combination with the structure of the CD69 fold known from X-ray analysis, verify the three-dimensional structure of the protein produced here with sufficient precision. Estimation of secondary structure content was done by least-squares analysis of FTIR amide I and II bands (Figure 1C) according to ref *36* and Raman amide I band according to ref *28*. The structure content determined by FTIR and Raman spectroscopy was in good agreement with the known crystal structure of the protein (Table 1). Values measured for the mutated proteins were virtually identical to those for the wild-type protein, indicating that no pronounced conformational changes occurred in the individual mutated proteins (Table 1). The standard deviation determined from the reference sets of protein spectra used in the methods similar to the circular dichroism spectroscopy was 8 and 5% for α-helical structures in FTIR and Raman spectroscopy, respectively. Whereas by vibrational spectroscopy helices are determined the least accurately, determination of the other structures is accurate to 4%. To further prove that the three-dimensional structure of mutant CD69 would be identical to that of the wild-type protein and remains stable during experiments performed here, we used several conformation-sensitive monoclonal antibodies. Their reactivities were identical for the wild-type and mutant proteins and remained stable even upon prolonged incubations at 37 °C (Table 2).

Table 1: Estimation of the Percent Composition of the Elements of Secondary Structure in Wild-Type and Mutated Monomeric CD69 Proteins

		crystal	FTIR	Raman	CD
CD69CWTY	α helix	21	16	25	22
	β sheet	36	33	38	35
	β turn	14	15	15	13
CD69CT1A	α helix	n.d.	17	n.d.[a]	23
	β sheet	n.d.	33	n.d.	34
	β turn	n.d.	14	n.d.	13
CD69CD1A	α helix	n.d.	16	n.d.	22
	β sheet	n.d.	32	n.d.	36
	β turn	n.d.	15	n.d,	14
CD69CK1A	α helix	n.d.	17	n.d.	23
	β sheet	n.d.	32	n.d.	34
	β turn	n.d.	15	n.d.	13
CD69CE1A	α helix	n.d.	16	n.d.	22
	β sheet	n.d.	32	n.d.	35
	β turn	n.d.	15	n.d.	13
CD69CE2A	α helix	n.d.	17	n.d.	21
	β sheet	n.d.	32	n.d.	34
	β turn	n.d.	15	n.d.	14
CD69CE3A	α helix	n.d.	18	n.d.	20
	β sheet	n.d.	34	n.d.	34
	β turn	n.d.	14	n.d.	15

[a] n.d., not determined.

Table 2: Thermal Stability of Wild-Type and Mutant Monomeric CD69 Probed by Immunoreactivity with Several Conformation-Sensitive Monoclonal Antibodies[a]

	T (°C)	MLR-3	Leu-23	BL-Ac/p26	BL-KFB/B1
CD69CWTY	4	4350[b] 53[c]	5573[b] 112[c]	7713[b] 253[c]	6017[b] 6172[c]
	37	4217[b] 47[c]	5078[b] 138[c]	7696[b] 210[c]	6210[b] 6237[c]
CD69CT1A	4	4438[b] 48[c]	5653[b] 123[c]	7619[b] 203[c]	6183[b] 6223[c]
	37	4175[b] 62[c]	5719[b] 134[c]	7715[b] 254[c]	6179[b] 6095[c]
CD69CD1A	4	4416[b] 51[c]	5637[b] 143[c]	7586[b] 238[c]	6219[b] 6179[c]
	37	4329[b] 55[c]	5775[b] 127[c]	7690[b] 237[c]	6208[b] 6188[c]
CD69CK1A	4	4478[b] 63[c]	5437[b] 128[c]	7663[b] 255[c]	6195[b] 6180[c]
	37	4491[b] 57[c]	5332[b] 132[c]	7730[b] 262[c]	6180[b] 6280[c]
CD69CE1A	4	4317[b] 60[c]	5456[b] 117[c]	7653[b] 247[c]	6223[b] 6312[c]
	37	4321[b] 55[c]	5660[b] 120[c]	7788[b] 253[c]	6312[b] 6330[c]
CD69CE2A	4	4378[b] 75[c]	5448[b] 121[c]	7324[b] 257[c]	6279[b] 6227[c]
	37	4322[b] 68[c]	5581[b] 135[c]	7712[b] 256[c]	6288[b] 6227[c]
CD69CE3A	4	4415[b] 72[c]	5651[b] 125[c]	7514[b] 264[c]	6213[b] 6218[c]
	37	4463[b] 70[c]	5328[b] 117[c]	7713[b] 264[c]	6213[b] 6218[c]

[a] Immunoreactivity expressed as cpm of the bound secondary antibodies averaged from triplicate experiments. [b] Native conditions. [c] Denaturing conditions.

Binding of Calcium by CD69. To determine how CD69CWTY binds calcium under physiological conditions, we saturated the purified protein with Ca^{2+} ions and performed direct determinations of calcium in the samples of protein after extensive dialyses (Figure 2A). In samples devoid of any protein or in samples dialyzed against acetate buffer at pH 3.5, rapid loss of calcium (in 2−3 h) from the retenate was evident. When the samples contained

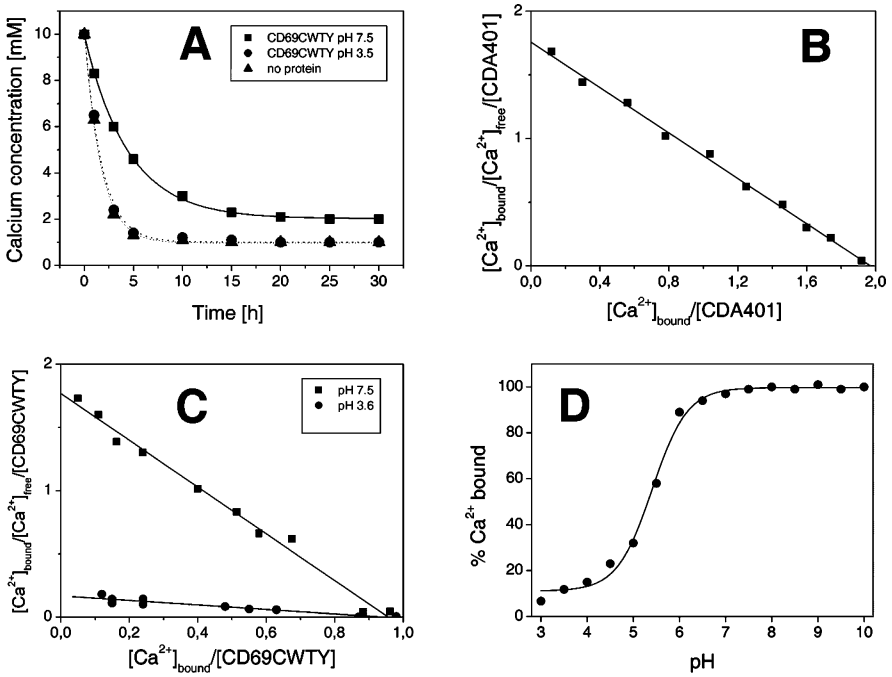

FIGURE 2: Binding of calcium by CD69CWTY is dependent on pH. (A) The capacity of CD69 to bind calcium was measured in samples of CD69CWTY saturated with calcium at neutral pH and then dialyzed extensively at pH 7.5 or 3.5. Calcium was also determined in a control sample devoid of proteins. Under neutral pH, approximately 1 mol of calcium was bound per 1 mol of protein. (B) Scatchard plot of the binding of $^{45}Ca^{2+}$ to dimeric CD69 determined at pH 7.5. (C) Scatchard plot of the binding of $^{45}Ca^{2+}$ to CD69CWTY determined at pH 7.5 and 3.6. (D) Capacity of CD69CWTY to bind calcium in buffers of varying pH. The affinity of $^{45}Ca^{2+}$ for this protein was related to that measured at pH 8 according to a formula % Ca^{2+} bound = [Ca^{2+}_{bound} (measured pH)/Ca^{2+}_{bound} (pH 8.0)] × 100.

CD69CWTY at pH 7.5, an equimolar amount of calcium remained bound to CD69 (Figure 2A).

More precise parameters for the binding of the calcium ion to CD69 were obtained from equilibrium dialysis studies using $^{45}Ca^{2+}$. Dimeric CD69 bound 2 mol of calcium per molecule with a K_d of approximately 54 μM (Figure 2B). Under neutral pH (7.5), the binding of calcium to monomeric CD69 was identical except that a single binding site was observed (Figure 2C). However, the affinity for calcium decreased under acidic pH (pH 3.6, K_d ~550 μM, Figure 2C). The complete pH dependence of binding of $^{45}Ca^{2+}$ (Figure 2D) resembles the pH-dependent titration curves of the carboxylic groups of acidic amino acids (aspartic and glutamic acid) in proteins and provides an initial indication that these amino acids may ligate calcium in CD69.

Calcium Is Ligated by Three Carboxyls of Asp 171, Glu 185, and Glu 187. To identify the amino acids in CD69 involved in calcium binding more precisely, a Conolly type surface with the electrostatic potential as surface property was generated for the published structure of this antigen (*19*). On this surface it was possible to identify a highly negatively charged region, which corresponded to a potential calcium-binding site. Calcium was then docked into this single site formed by aspartic acid Asp 171 and the two adjacent glutamic acids Glu 185 and Glu 187 (Figure 3). Remarkably, the insertion of calcium into this site resulted in no significant changes in the overall three-dimensional structure of CD69. The open conformation of the carboxyls of the above amino acids (Figure 3, yellow residues) closed up into the coordination sphere of the ligated calcium atom (Figure 3, green residues) thus joining two protein loops. More importantly, the conformational change in the amino acids ligating calcium resulted in a dramatic change in the conformation of Lys 172 (shown in purple and blue in the calcium-free and calcium-containing form of the protein, respectively—Figure 3) in one of these loops and of Thr 107 (not shown) in the second loop. The presence of a lysine residue close to the three negatively charged amino acids coordinating the ion is a binding motif known from P-type ATPases and other proteins containing a Rossman fold, where the positive charge of the lysine may supply charge shielding and stabilization during phosphorylation (*37*).

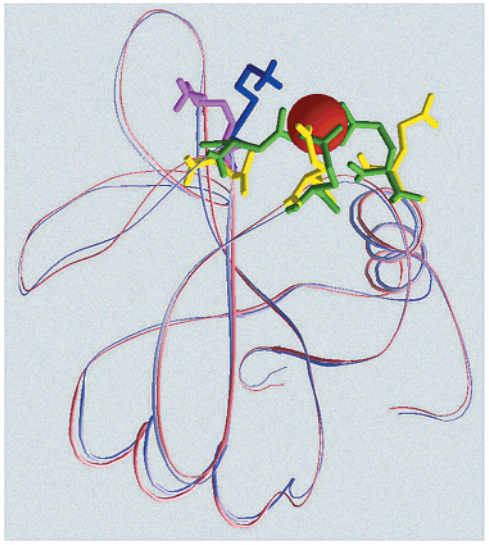

FIGURE 3: Docking of Ca^{2+} into the crystal structure of CD69. Binding of calcium to CD69 results in the structural rearrangement of Asp 171 (left), Glu 185 (middle), and Glu 187 (right) resulting in the conformational change of the protein from calcium open (yellow) to calcium closed (green) configuration. Concomitant with these changes, a dramatic shift in the position of lysine (violet in the open and blue in the closed configuration) was observed, as well as a minor shift in the structure of the C-type lectin domain backbone (thin red and thin blue lines, respectively).

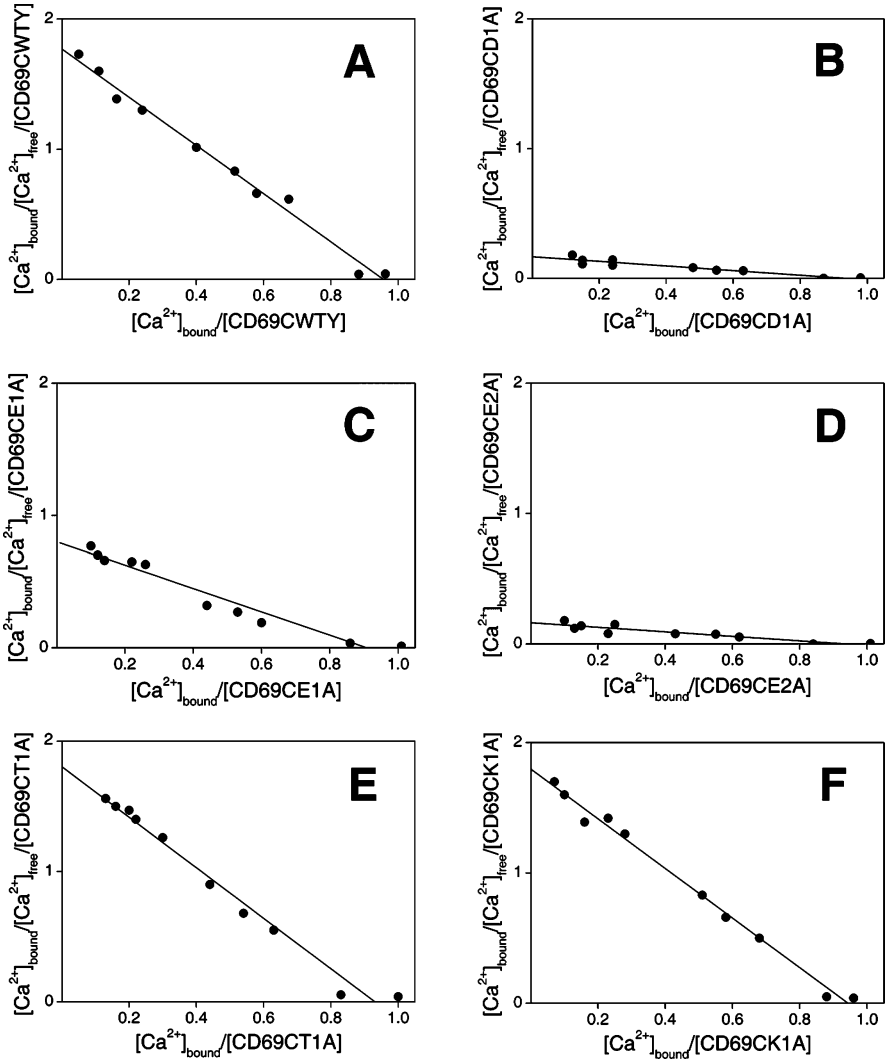

FIGURE 4: Scatchard plots of the binding of ^{45}Ca by wild-type CD69 and mutant CD69 proteins altered in amino acids surrounding the predicted calcium-binding site. The binding of $^{45}Ca^{2+}$ was measured to the proteins indicated at the individual panels.

To prove the role of the above amino acids in the binding of calcium, mutant proteins have been produced in which the above amino acids (i.e., Asp 171, Glu 185, and Glu 187) have been individually replaced by alanine (Figure 1A, CD69CD1A, CD69CE1A, and CD69CE2A, respectively). Results of the direct binding of calcium to wild-type and mutant proteins performed at neutral pH are presented in Figure 4. The binding of calcium to the wild-type protein proceeded with a dissociation constant of approximately 54 μM. Mutation of any of the anticipated carboxyl groups of Asp 171, Glu 185, or Glu 187 resulted in a considerable reduction of the affinity of calcium binding (K_d of 0.5, 0.1, and 0.5 mM has been estimated for CD69CD1A, CD69CE1A, and CD69CE2A, respectively, Figures 4B−D), although the effect observed for Glu 185 has been somewhat less profound. The double mutant with Glu 185 and Glu 187 replaced by alanine exhibited totally no binding of calcium (results not shown). On the other hand, mutating Thr 107 or Lys 172, two residues in close proximity of the calcium-binding site, did not cause any significant change in the affinity for calcium (K_d for CD69CT1A and CD69CK1A have been estimated as 52 and 53 μM, respectively, Figure 4E,F).

Calcium Binding Creates a High-Affinity Site for GlcNAc. Since the above data provided clear evidence that calcium is an integral component of CD69 protein under physiological conditions, and since there have been no changes in the overall structure of the protein except in the spatial position of specific amino acid residues, we were interested in investigating the effects of calcium binding by CD69 on the interaction with the carbohydrate ligands. Since the most precise and correct method to address these issues would be a direct-binding assay, we decided to perform equilibrium dialysis experiments with the labeled carbohydrates. GlcNAc, reported previously as the best monosaccharide ligand for CD69 (*21*), is available in ^3H labeled form from commercial sources. However, this compound is represented as a mixture of an α and β anomeric form, the ratio of which depends on the composition of the solvent. The anomeric composition of GlcNAc in equilibrium is 67% α pyranose, 32% β pyranose, and there is less than 1% of the furanose forms (*38*). Should any of these anomers bind better to CD69CWTY, the results of the direct-binding assays will be distorted. To check this possibility, we employed an inhibition assay and have compared the affinity of interaction of GlcNAc together with both its methyl glycosides in which the specific anomeric conformation is fixed by methylation. We have found that the inhibitory potency of these three carbohydrates are essentially identical ($IC_{50} = 6 \times 10^{-3}$ M) thus providing

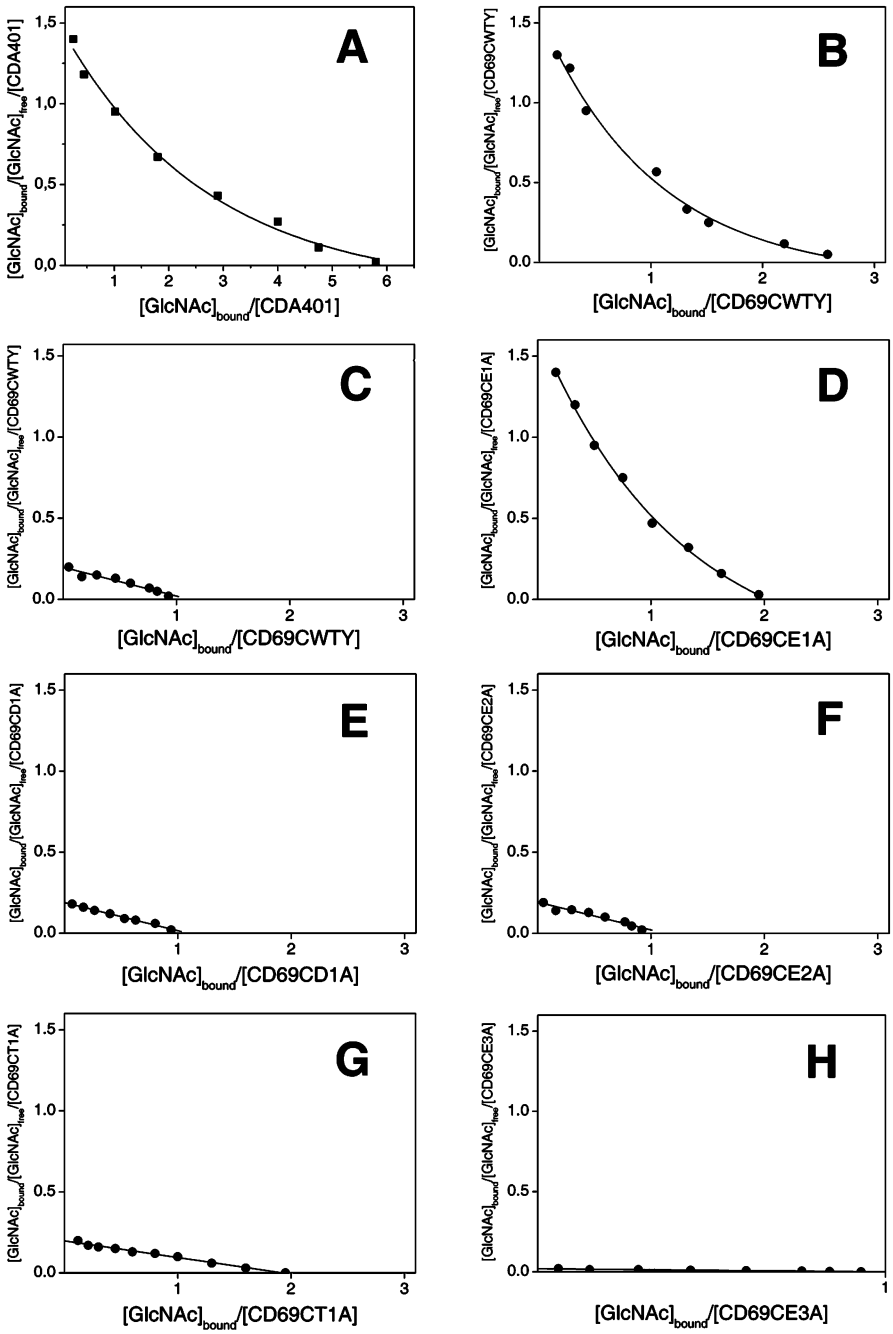

FIGURE 5: Binding of GlcNAc to CD69 is dramatically dependent on the calcium status of the protein. (A) Scatchard plot of the binding of [^{3}H]-GlcNAc to dimeric CD69. (B) Scatchard plot of the binding of [^{3}H]-GlcNAc to CD69CWTY in the presence of calcium. (C) Scatchard plot of the binding of [^{3}H]-GlcNAc to CD69CWTY decalcified by dialysis against acidic buffer (pH 3.6). (D−G) Scatchard plots of the binding of [^{3}H]-GlcNAc to various calcium-containing CD69 mutants. Amino acids predicted to be important for the carbohydrate binding were mutated to alanine. (H) Scatchard plot of the binding of [^{3}H]-GlcNAc to CD69CE3A decalcified by dialysis against acidic buffer (pH 3.6).

an important justification for the use of the GlcNAc in further experiments.

When we measured the binding of the radiolabeled GlcNAc to dimeric CD69, the binding curve was nonlinear indicating the existence of several types of binding sites (Figure 5A). Nevertheless, it was obvious that the dimeric protein bound 6 mol of GlcNAc per mol of protein, while the monomeric CD69 bound only 3 mol (cf. Figure 5A,B). However, the binding of GlcNAc to CD69CWTY changed dramatically in the absence of calcium. In CD69CWTY from which calcium had been removed by dialysis in acidic (pH 3.5) buffer (reversibility of this decalcification was demonstrated by Bezouška et al. (*21*)), only a single, low-affinity (K_d = 0.5 mM) binding site was observed (Figure 5C).

Structural Model for GlcNAc Binding and Its Experimental Verification. It would appear from the above results that three binding sites for GlcNAc of unequal affinity exist in one ligand-binding domain of CD69. Considering this number of binding sites, and the precision with which the data presented in Figure 5B can be determined, no mathematical calculation would be able to estimate the contributions made by the individual binding sites. Therefore, we addressed the problem using molecular modeling followed by site-directed mutagenesis. We have used the structure of the calcium-

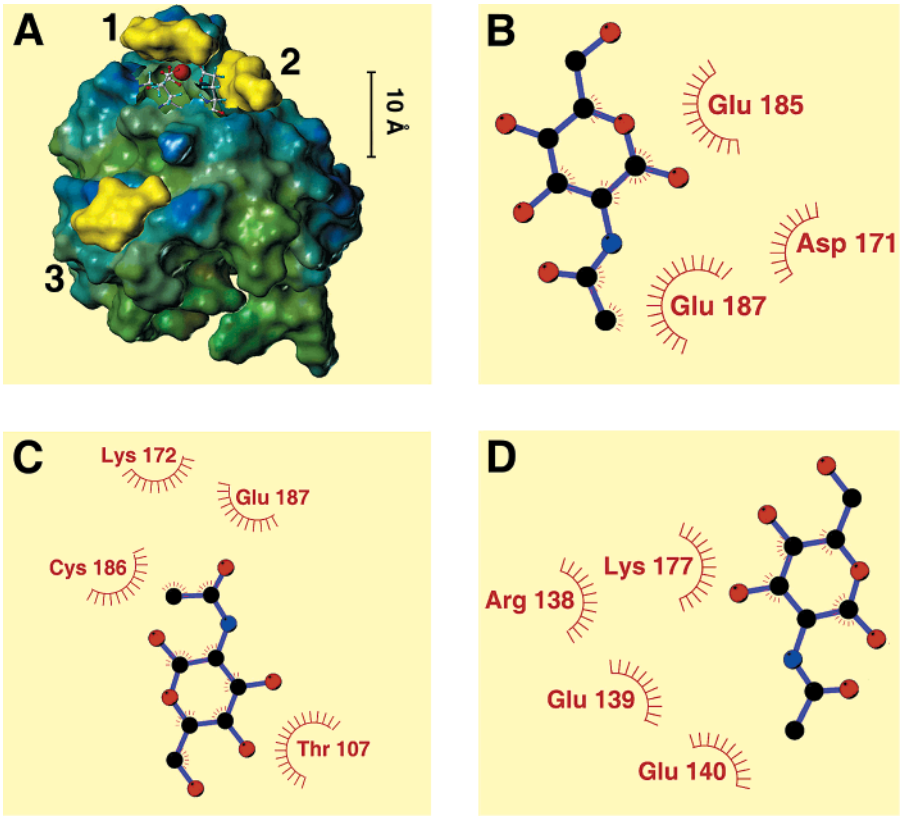

FIGURE 6: Docking of GlcNAc into the calcium-containing form of CD69. (A) Molecular details of the three GlcNAc molecules docked into the calcium form of CD69. The potential high-affinity binding site (site 2) is localized close to the calcium-binding site. One low-affinity binding site (site 1) is also close to the calcium ion, while the second low-affinity binding site (site 3) is in the more distal part of the molecule. (B−D) The localization of the respective binding sites for GlcNAc is described in more detail. In these panels, the amino acids involved in the interactions with the specific atoms of the monosaccharide structures are indicated.

ligating form of the protein and performed molecular docking of the carbohydrate into the receptor structure. According to this model, GlcNAc bound into three sites, designated 1, 2, and 3 (Figure 6A). Detailed presentation of these three sites (sites 1−3) reveals the key amino acid residues involved in the ligation of the three *N*-acetylglucosamines (Figure 6B−D, respectively).

Interestingly, in site 1 (Figure 6B) the same amino acids shown to ligate calcium seem to participate. Therefore, when mutating these amino acids one should consider the already described effect on the binding of calcium (Figure 4) that has itself a dramatic influence on GlcNAc binding—the loss of two binding sites for GlcNAc and the dramatic decrease of the affinity to this carbohydrate (Figure 5C). From this point of view, mutating Asp 171 or Glu 187 to Ala would cause the loss of calcium, and the effects on binding of GlcNAc would thus be predicted to parallel the effect of decalcification. Indeed, binding experiments performed with these mutants provided a curve identical to the decalcified protein (compare Figure 5E,F to C). Mutation of Glu 185 to Ala did not dramatically decrease the binding of calcium (see Figure 4C) and can thus serve as a better indicator of amino acid defining the site 1. Binding of GlcNAc to this mutant is characterized by the clearly visible loss of one binding site while retaining most of the binding affinity. This would indicate that site 1 that has been knocked out by Glu185 mutation has relatively low affinity for GlcNAc.

Amino acids ligating the GlcNAc in site 2 are shown in Figure 6C; Glu 187 is a common amino acid for both sites 1 and 2. Of the amino acids defining the site 2 more specifically, both Thr 107 and Lys 172 were mutated to Ala. As has been demonstrated in Figure 4, these mutations have no effect on the binding of calcium by CD69. However, both of these mutants drastically decreased the binding affinity for GlcNAc with the concomitant loss of one binding site (shown for Thr in Figure 5G, the data for the Lys mutant were identical). Therefore, we can conclude that site 2 is the high-affinity binding site for GlcNAc. The approximately linear shape of the Scatchard plot in Figure 5G indicates similar affinity for the binding of GlcNAc in sites 1 and 3 (K_d approximately 1 mM). On the other hand, by comparison of data in Figure 5B,E,G we may estimate that the K_d for GlcNAc binding to site 2 is approximately 63 μM. In the case of the double mutant (Glu 185 and Glu 187 replaced by Ala, results not shown), the situation was the same as in the case of decalcified protein. Only one GlcNAc binding site with low affinity remained.

Binding site 3 is defined by amino acids Arg 138, Glu 139, Glu 140, and Lys 177. This site is not dependent on the binding of calcium, and the affinity of GlcNAc for this site can thus be estimated either from binding in the absence of calcium (Figure 5C) or from binding to mutants causing the loss of this ion (Figure 5E,F). When we mutate Glu 139, and perform binding to the decalcified form of this mutant, essentially all of the GlcNAc binding is lost (Figure 5H). This is another independent confirmation of the number of binding sites. In the case of the double mutant with Glu 185 and Glu 187 replaced by alanine, only one calcium-binding site rested, and results (not shown) are practically identical to Figure 5C—decalcified protein. Thus, summarizing the

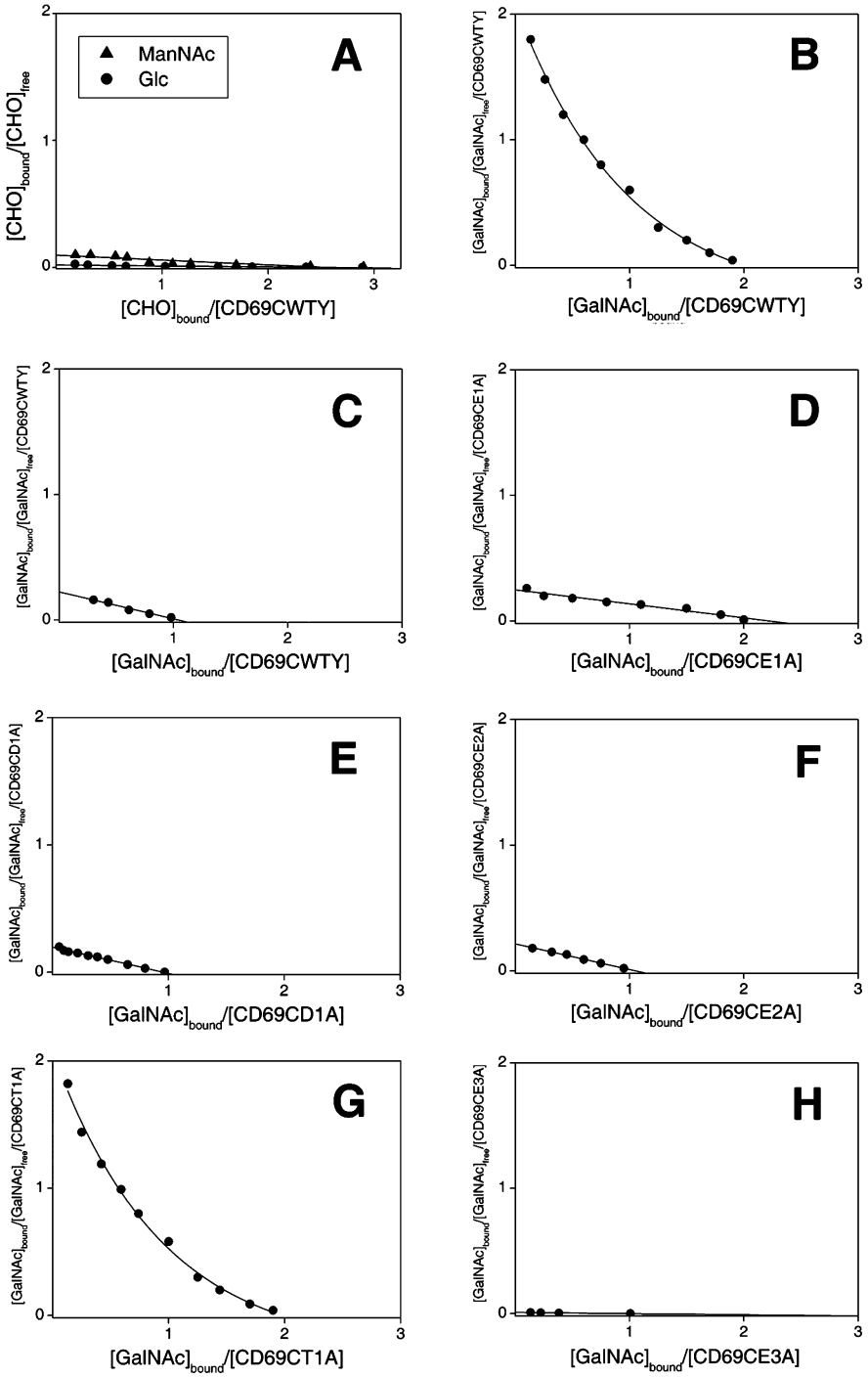

FIGURE 7: Additional *N*-acetylhexosamines differ from GlcNAc in a number of binding sites and their affinities. (A) Scatchard plot of the binding of [^{3}H]-ManNAc and [^{3}H]-glucose to CD69CWTY. (B) Scatchard plot of the binding of [^{3}H]-GalNAc to CD69CWTY. (C) Scatchard plot of the binding of [^{3}H]-GalNAc to CD69CWTY decalcified by dialysis against acidic buffer (pH 3.6). (D−G) Scatchard plots of the binding of [^{3}H]-GalNAc to various calcium-containing CD69 mutants. Amino acids predicted to be important for the carbohydrate binding were mutated to alanine. (H) Scatchard plot of the binding of [^{3}H]-GalNAc to CD69CE3A decalcified by dialysis against acidic buffer (pH 3.6).

results from the site-directed mutagenesis, we can map out the position and affinity of GlcNAc-binding sites.

Equilibrium Binding of Glucose and N-Acetylated Hexosamines Supports the Structural Model. To verify the model and predictions from the computer docking, we have performed additional binding experiments. Essentially no binding of the nonacetylated carbohydrate glucose to CD69 could be recorded (Figure 7A), indicating the important contribution of the acetamido group to the binding specificity of the CD69 receptor. *N*-Acetyl-D-mannosamine, a carbohydrate shown previously to have a remarkably high affinity for rat NKR-P1A receptor—another member of the group V of C-type animal lectins (*13*, *39*)—was bound extremely poorly by CD69 (Figure 7A). This represents another important argument for the validity of our structural model that strictly requires the equatorial arrangement of the 2-acetamido group in carbohydrates bound to sites 1, 2, or 3.

More subtle structural alterations of the GlcNAc ligand can result in another, and somewhat unexpected, mode of

carbohydrate interaction with CD69. Here, GalNAc, which had been shown in previous experiments to be a good ligand for CD69, bound in two binding sites with the affinity similar to GlcNAc (Figure 7B). When binding of radiolabeled GalNAc was inhibited by an excess of nonlabeled GlcNAc, essentially all binding could be eliminated confirming that GalNAc shares with GlcNAc identical binding sites in CD69. To investigate which of the three binding sites for GlcNAc corresponds to the two binding sites for GalNAc, we measured the binding to mutated CD69 proteins. When equilibrium binding was performed with the protein from which the calcium had been chemically removed, only the low-affinity binding site was preserved (Figure 7C), indicating that one of the calcium-dependent sites for GlcNAc binding (sites 1 or 2, Figure 6A) also represents the high-affinity site for GalNAc. This conclusion was further supported by binding to Asp 171 and Glu 187 mutants that provide Scatchard plots identical to that of the decalcified protein (Figure 7E,F, respectively). Binding of GalNAc to Thr 107 and Lys 172 mutants was identical to that of the wild-type calcium-containing protein (shown in Figure 7G for the threonine mutant), indicating that the binding site 2 is not the high-affinity site for GalNAc. This conclusion was further supported by a prediction from the molecular model indicating that GalNAc with its axial C4 hydroxyl would not dock into the binding site 2. On the other hand, a high-affinity docking would be suggested for GalNAc by the molecular model in the case of GlcNAc-binding site 1. In this case, the axial C4 hydroxyl of the former carbohydrate would be expected to establish a strong interaction with Glu 185 rather then just with the aqueous environment as was typical for the latter carbohydrate. The next experimental evidence for this type of interaction was clearly provided by the CD69CE1A mutant, which displayed a remarkable reduction in affinity assigned to the high-affinity site (Figure 7D). As in the case of GlcNAc binding, the calcium distal-binding site 3 (Figure 6A) seems also to represent the low-affinity site for GalNAc as evident from the total loss of GalNAc binding in the case of the CD69C3A mutant examined in its calcium-depleted form (Figure 7H).

CONCLUSION

Our work provides an important formal proof for the existence of one calcium-binding site formed by Asp 171, Glu 185, and Glu 187 in the lectin domain of the CD69 molecule. It reveals a novel type of the Ca^{2+} binding that differs from the one described for the relative protein—MBP (*40*). It should be pointed out that Asp 171 is the only conserved amino acid that is shared with the calcium-binding site in MBP. Thus, it appeared that calcium binding in the group V of C-type lectin receptors can be more variable than was originally believed. This binding could not be observed in the published crystal structures (*19*, *20*) based on proteins produced in calcium-free form. Moreover, dialysis of the protein against buffer containing a physiological concentration of calcium at neutral pH provided clear evidence for biologically relevant binding of this ion.

The identification of binding sites for *N*-acetyl hexosamines (three for GlcNAc and two for GalNAc) that could be clearly dissected based on site-directed mutagenesis data (together with the elucidation of the role of calcium in the binding process) sheds a light onto the current controversy about the carbohydrate-binding specificity of this protein (*21*, *22*). The high-affinity binding site for GlcNAc (Figure 6C) has certain unique features not observed in other C-type animal lectins. According to the results of the molecular docking, no direct interaction between the calcium ion and the carbohydrate could be observed. Interestingly, the high-affinity binding site for GalNAc was different from that for GlcNAc. It is evident that our findings are essential to understand the nature of these discrepancies. The unknown electron density in the Natarajan et al.'s crystal (*20*) of hexagonal, pyranose-like shape is localized directly in the position of the carbohydrate-binding site 1 described in our work. Moreover, the arrangement of all three carbohydrate-binding sites detected here is in a good agreement with the suggestion of Llera et al.'s ligand-binding surface (sites 1 and 3 are directly in this area, and site 2 is in close proximity (*19*)).

From the definition of the protein domain as an independent functional module, one would expect that it should be possible to obtain them as physically separable entities and engage into their detailed structural studies. However, there is evidence that this may not always be the case. In particular, within the C-type lectins family, there are examples of protein in which truly independent modules exist (e.g., antigen CD23 (*12*)), while there is a strong cooperativity between the carbohydrate-binding domains in the case of other proteins, such as MBP (*40*). From the calcium and monosaccharide-binding data presented here, we can clearly conclude that all binding sites for these compounds are located exclusively in the globular ligand-binding domain of CD69 (*12*) defined by a polypeptide encompassing amino acids Ser100 to Lys199; no additional binding sites for these ligands in other part of the molecule, such as the stalk and neck regions, could be detected. Both ligand-binding domains in the dimeric protein seem to bind the above ligands independently, and there is very little cooperativity for binding between them. Altogether, identification of binding sites for calcium and monosaccharides now opens the way for the search for complex oligosaccharides as the potential physiological ligands. Although the exact mode of binding of the complex carbohydrates to CD69 remains to be clarified in future studies, our description of the individual sugar-binding sites provides an important basis for such investigations. From a point of view of general biochemistry, it is interesting to observe how the interaction of small ions with proteins may result in minor structural changes that eventually lead to specific interactions important for the recognition events within the immune system.

ACKNOWLEDGMENT

We thank Tomáš Semeňuk for a gift of methyl-α-2-deoxy-2-acetamido-D-glucopyranoside, Petr Sedmera for NMR analysis of the monosaccharides, Kateřina Hofbauerová for her help with the evaluation of the spectral data, Kvido Stříšovský for advice on site-directed mutagenesis, and one of the reviewers for many helpful suggestions.

REFERENCES

1. Testi, R., D'Ambrosio, D., De Maria, R., and Santoni, A. (1994) *Immunol. Today 15*, 479−483.
2. Testi, R., Phillips, J. H., and Lanier, L. L. (1988) *J. Immunol. 141*, 2557−2563.

3. De Maria, R., Cifone, M. G., Trotta, R., Rippo, M. R., Festuccia, C., Santoni, A., and Testi, R. (1994) *J. Exp. Med. 180*, 1999−2004.
4. Gavioli, R., Risso, A., Smilovich, D., Baldissarro, I., Capra, M. C., Bargellesi, A., and Cosulich, M. E. (1992) *Cell Immunol. 142*, 186−196.
5. Bieber, T. (1994) *Immunol. Today 15*, 52−53.
6. Testi, R., Pulcinelli, F., Frati, L., Gazzaniga, P. P., and Santoni, A. (1990) *J. Exp. Med. 172*, 701−707.
7. Risso, A., Smilovich, D., Capra, M. C., Baldissarro, I., Yan, G., Bargellesi, A., and Cosulich, M. E. (1991) *J. Immunol. 146*, 4105−4114.
8. Gerosa, F., Tommasi, M., Scardoni, M., Accolla, R. S., Pozzan, T., Libonati, M., Tridente, G., and Carra, G. (1991) *Mol. Immunol. 28*, 159−168.
9. Hamann, J., Fiebig, H., and Strauss, M. (1993) *J. Immunol. 150*, 4920−4927.
10. Lopez-Cabrera, M., Santis, A. G., Fernandez-Ruiz, E., Blacher, R., Esch, F., Sanchez-Mateos, P., and Sanchez-Madrid, F. (1993) *J. Exp. Med. 178*, 537−547.
11. Ziegler, S. F., Ramsdell, F., Hjerrild, K. A., Armitage, R. J., Grabstein, K. H., Hennen, K. B., Farrah, T., Fanslow, W. C., Shevach, E. M., and Alderson, M. R. (1993) *Eur. J. Immunol. 7*, 1643−1648.
12. Sancho, D., Santis, A. G., Alonso-Lebrero, J. L., Viedma, F., Tejedor, R., and Sánchez-Madrid, F. (2000) *J. Immunol. 165*, 3868−3875.
13. Bezouška, K. (1996) *Biochem. Soc. Trans. 24*, 156−161.
14. Weis, W. I., Taylor, M. E., and Drickamer, K. (1998) *Immunol. Rev. 163*, 19−34.
15. Boyington, J. C., Riaz, A. N., Patamawenu, A., Coligan, J. E., Brooks, A. G., and Sun, P. D. (1999) *Immunity 10*, 75−82.
16. Tormo, J., Natarajan, K., Margulies, D. H., and Mariuzza, R. A. (1999) *Nature 402*, 623−631.
17. Bezouška, K. (2001) *J. Biotech. 90*, 269−290.
18. Bajorath, J., and Aruffo, A. (1994) *J. Biol. Chem. 269*, 32457−32463.
19. Llera, A. S., Viedma, F., Sanchez-Madrid, F., and Tormo, J. (2001) *J. Biol. Chem. 276*, 7312−7319.
20. Natarajan, S., Sawicki, M. W., Margulies, D. H., and Mariuzza, R. A. (2000) *Biochemistry 39*, 14779−14786.
21. Bezouška, K., Nepovím, A., Horváth, O., Pospíšil, M., Hamann, J., and Feizi, T. (1995) *Biochem. Biophys. Res. Commun. 208*, 68−74.
22. Childs, R. A., Galustian, C., Lawson, A. M., Dougan, G., Benwell, K., Frankel, G., and Feizi, T. (1999) *Biochem. Biophys. Res. Commun. 266*, 19−23.
23. Evans, E. A., Sheppard, H. C., Turner, J. C., and Warrel, D. C. (1974) *J. Labeled Compounds 10*, 569−587.
24. Valez-Gomez, M., Reyburn, H. T., Mandelboim, M., and Strominger, J. L. (1998) *Immunity 9*, 337−344.
25. Laemmli, U. K. (1970) *Nature 227*, 680−685.
26. Bezouška, K., Sklenář, J., Novák, P., Halada, P., Havlíček, V., Kraus, M., Tichá, M., and Jonáková, V. (1999) *Protein Sci. 8*, 1551−1556.
27. Dousseau, F., Therrien, M., and Pézolet, M. (1989) *Appl. Spectrosc. 43*, 538−542.
28. Williams, R. W. (1986) *Methods Enzymol. 130*, 311−331.
29. Bezouška, K., Vlahas, G., Horváth, O., Jinochová, G., Fišerová, A., Giorda, R., Chambers, W. H., Feizi, T., and Pospíšil, M. (1994) *J. Biol. Chem. 269*, 16945−16952.
30. Piskarev, V. E., Navrátil, J., Karásková, H., Bezouška, K., and Kocourek, J. (1990) *Biochem. J. 270*, 755−760.
31. Rosenthal, H. E. (1967) *Anal. Biochem. 20*, 525−532.
32. Clark, M., Cramer, R. D., and Van Opdenbosch, N. (1989) *J. Comput. Chem. 10*, 982−1012.
33. Gasteiger, J., and Marsili, M. (1980) *Tetrahedron 36*, 3219−3238.
34. Morris, G. M., Goodsell, D. S., Halliday, R. S., Huey, R., Hart, W. E., Belew, R. K., and Olson, A. J. (1998) *J. Comput. Chem. 19*, 1639−1662.
35. Solis, F. J., and Wets, R. J. B. (1981) *Math. Oper. Res. 6*, 19−30.
36. Dousseau, F., and Pézolet, M. (1990) *Biochemistry 29*, 8771−8779.
37. Ettrich, R., Melicherčík, M., Teisinger, J., Ettrichová, O., Krumscheid, R., Hofbauerová, K., Kvasnička, P., Schoner, W., and Amler, E. (2001) *J. Mol. Model. 7*, 184−192.
38. Angyal, S. J. (1984) *Adv. Carbohydr. Chem. Biochem. 42*, 15−68.
39. Krist, P., Herkommerová-Rajnochová, E., Rauvolfová, J., Semeňuk, T., Vavrušková, P., Pavlíček, J., Bezouška, K., Petrus, L., and Křen, V. (2001) *Biochem. Biophys. Res. Commun. 287*, 11−20.
40. Weis, W. I., Drickamer, K., and Hendrickson, W. A. (1992) *Nature 360*, 127−134.

BI027298L